# Peroxiredoxin IV plays a critical role in cancer cell growth and radioresistance through the activation of the Akt/GSK3 signaling pathways

Na Ding[1], Hong Jiang[1], Pratik Thapa[1], Yanning Hao[1], Aziza Alshahrani[1], Derek Allison[2], Tadahide Izumi[1], Vivek M. Rangnekar[3], Xiaoqi Liu[1,3], and Qiou Wei[1,3,*]

From the [1]Department of Toxicology and Cancer Biology, [2]Pathology and Laboratory Medicine, and [3]Markey Cancer Center, University of Kentucky, Lexington, Kentucky, USA

Edited by Eric Fearon

High levels of redox enzymes have been commonly observed in various types of human cancer, although whether and how the enzymes contribute to cancer malignancy and therapeutic resistance have yet to be understood. Peroxiredoxin IV (Prx4) is an antioxidant with bona fide peroxidase and molecular chaperone functions. Here, we report that Prx4 is highly expressed in prostate cancer patient specimens, as well as established prostate cancer cell lines, and that its levels can be further stimulated through the activation of androgen receptor signaling. We used lentivirus-mediated shRNA knockdown and CRISPR-Cas9 based KO techniques to establish Prx4-depleted prostate cancer cells, which showed delayed cell cycle progression, reduced rate of cell proliferation, migration, and invasion compared to control cells. In addition, we used proteome profiler phosphokinase arrays to identify signaling changes in Prx4-depleted cells; we found that loss of Prx4 results in insufficient phosphorylation of both Akt and its downstream kinase GSK3α/β. Moreover, we demonstrate that Prx4-depleted cells are more sensitive to ionizing radiation as they display compromised ability to scavenge reactive oxygen species and increased accumulation of DNA damage. In mouse xenograft models, we show depletion of Prx4 leads to significant suppression of tumor growth, and tumors formed by Prx4-depleted cells respond more effectively to radiation therapy. Our findings suggest that increased levels of Prx4 contribute to the malignancy and radioresistance of prostate cancer through the activation of Akt/GSK3 signaling pathways. Therefore, strategies targeting Prx4 may be utilized to potentially inhibit tumor growth and overcome radioresistance in prostate cancer.

Prostate cancer is the most prevalent diagnosed cancer in men, and patients with localized prostate cancer are often treated with radical prostatectomy, radiation therapy, or the combination of both (1–3). In 2019, there were more than 3.6 million men with the diagnosis of prostate cancer in United States (2). Even with the commonly accepted screening of prostate-specific antigen (PSA) levels for early diagnosis, prostate cancer is still the second leading cause of cancer death in men (1, 4). For advanced disease, androgen deprivation therapy, chemotherapy, bone-directed therapy (such as zoledronic acid or denosumab), radiation, or the combination of these treatments may be used (2). Radiation, either alone or combined with other therapies, is still the most common strategy to treat both localized and advanced prostate cancer. However, half of the patients who have been treated with salvage radiation will eventually suffer from disease progression, particularly those with aggressive features when it was first diagnosed (5, 6). Radiotherapy directly causes DNA damages and cell death through massive generation of reactive oxygen species (ROS) (6, 7). However, radiation also inevitably causes damages to surrounding normal tissue as side effects even with modulated doses (7). Therefore, identifying an effective strategy to sensitize prostate cancer to radiotherapy will improve the efficacy of current therapies and reduce radiation-associated side effects.

Peroxiredoxin (Prx) is a family of highly conserved peroxidases that scavenge hydrogen peroxide ($H_2O_2$) as well as contribute to ROS signaling under physiological conditions (8). Prx can maintain local redox homeostasis and regulate ROS signaling pathway, which involves the oxidation of various downstream target proteins. Mammalian cells express six members of Prx (from Prx1 to Prx6), which can be divided into three subgroups (2-Cys, atypical 2-Cys, and 1-Cys Prx) based on the presence/absence and the location of the resolving cysteine ($C_R$) (8, 9). The 2-Cys Prxs reacts with $H_2O_2$ through its peroxidatic Cys ($C_P$), leading to the formation of disulfide bonds with the spatially adjacent $C_R$ to establish head–tail type of homodimers or heterodimers. If the level of $H_2O_2$ accumulates, both $C_R$ and Cp can be overoxidized to sulfinic ($-SO_2$) and/or sulfonic ($-SO_3$) forms (8). The overoxidized Prxs can multimerize into a ring structure with high molecular weight, which functions as protein chaperone to facilitate protein folding and prevent protein aggregation (10). Among the family of Prxs, Prx4 is the only one located in endoplasmic reticulum (ER), where the level of ROS is believed to be the highest among all subcellular organelles (8, 11). The imbalance of ER redox homeostasis will cause ER stress and

the activation of the unfolded protein response (11). Previous studies indicate that Prx4 is upregulated in different types of human cancer, including glioma (12, 13), lung cancer (14), leukemia (15), prostate cancer (16), colorectal cancer (17), and multiple myeloma (18). In the context of carcinogenesis, Prx4 promoted urethane-induced lung cancer through the increased phosphorylation of NF-κB p65 and c-Jun in transgenic mouse model study (19). In prostate cancer, the most common metastatic site is the bone, which is often the only clinically detectable site of metastasis (20), and depletion of Prx4 in prostate cancer cells can reduce the number of osteolytic lesions by inhibiting the differentiation of osteoclast (21). However, the mechanism of how Prx4 contributes to prostate cancer malignancy is still not completely understood.

In this study, our goal is to evaluate the expression of Prx4 in human prostate cancer and to study whether and how Prx4 contributes to prostate cancer development and therapeutic resistance. We examined the expression levels of Prx4 in multiple prostate cell lines as well as patient normal and tumor specimens. Cell lines with or without the expression of Prx4 were established, and phenotypic changes associated with the presence or absence of Prx4 were studied, and findings from cell culture were further confirmed in mouse models. In addition, molecular mechanisms by which Prx4 contributes to cancer malignancy and radioresistance were determined through series of biochemical analysis. Our data demonstrate that Prx4 plays a critical role in prostate cancer development and can be used as a potential target to improve the efficacy of radiation therapy in prostate cancer patients.

## Results

### Meta-analysis indicates the amplification of PRDX4 *gene and increased transcripts in human prostate cancer patients*

Prx4 is encoded by the gene *PRDX4* on chromosome X in mammals. To study the functional significance of Prx4 in the pathogenesis of human cancer, meta-analysis was used to examine *PRDX4* gene alterations in cancer patients. When *PRDX4* was input as the query gene in all curated set of

nonredundant studies in cBioPortal database (currently containing 150,839 samples from 145,223 patients), we found that prostate cancer has the highest rate of gene alterations among all cancer types. In particular, the alteration is predominantly characterized as gene amplification in all prostate cancer cases collected from five different cohorts of prostate cancer studies (Fig. 1A). In this analysis, gene amplification means an increased copy number of the gene in its original foci. For example, 10 out of 61 samples have *PRDX4* gene amplification in metastatic prostate adenocarcinoma study reported from Arul Chinnaiyan's and Scott Tomlins' labs at the University of Michigan (22), 20 out of 154 samples are amplified in prostate adenocarcinoma study reported from Fred Hutchinson cancer center (23), 48 out of 444 samples in metastatic prostate adenocarcinoma study reported by the SU2C/PCF Dream Team (24), and 10 out of 150 samples in metastatic prostate cancer reported by the same team (25). In contrast to the high rate of amplification, mutations of *PRDX4* gene are very rare in prostate cancer but can be found in tumors of other tissues/organs. In the current cBioPortal database, there are 91 mutations in *PRDX4* gene identified, including 73 missense mutations at nonoverlapping site, six nonsense mutations, 11 mutations that may affect splicing, and one that may create a new fusion mutant. It appears that these mutations occurred randomly at extremely low frequency since no hotspot mutations were identified (Fig. S1A). Moreover, a close examination of these mutation sites reveals that none of these mutations is predicted to affect Prx4 enzymatic activity based on previously published structural studies (26). We also examined *PRDX4* copy number variations and found significant increase in the numbers of gain and amplification (Fig. S1B). In addition, methylation levels of *PRDX4* gene promoter in various cancers and normal tissues were compared, and we found that it is significantly decreased in prostate cancer compared with normal prostate (Fig. S1C). In consistence, transcript levels of Prx4 are significantly increased in a variety of human tumors including prostate cancer compared with their levels in normal tissues (Fig. S1D). When prostate cancer patient samples at different stages were compared, the levels of *PRDX4*
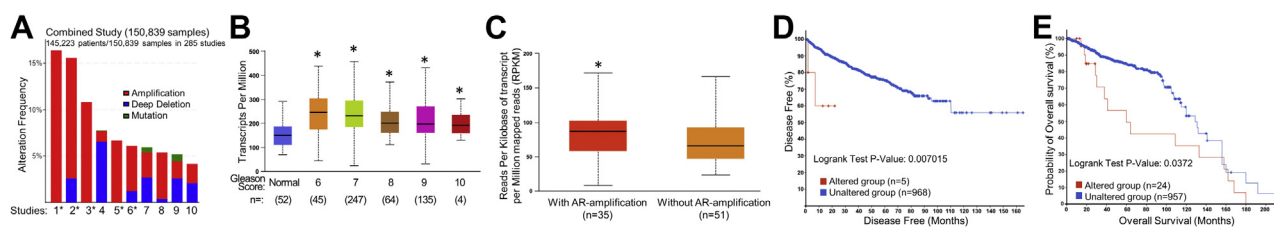


**Figure 1. Evaluation of *PRDX4* gene alterations, transcript levels, and their correlation with prognosis in patients with all types of tumors through meta-analysis of multiple existing datasets as of April 2022.** *A*, top 10 studies with high frequency of *PRDX4* gene alterations. Data were summarized from a total of 145,223 patients/150,839 samples in 285 studies (cBioPortal). *Prostate cancer studies and citation sources are #1: metastatic prostate adenocarcinoma (59); #2: prostate adenocarcinoma (23); #3: metastatic prostate adenocarcinoma (24); #5: metastatic prostate cancer (25); #6: the metastatic prostate cancer project (22). Other cancer studies and citations sources are #4: pan-cancer analysis of whole genomes (60); #7: esophageal carcinoma (TCGA, Firehose Legacy); #8: sarcoma (TCGA, Firehose Legacy); #9: esophageal carcinoma (61); #10: diffuse large B-cell lymphoma (TCGA, PanCancer Atlas). Amplification indicates a high-level gain of more than a few copies of the gene. Deep deletion indicates a deep loss, possibly a homozygous deletion. *B*, the levels of *PRDX4* gene transcript in various stages of prostate cancer compared with normal prostate. Data were obtained from the TCGA RNA-Seq data (compared with control, *$p < 0.05$, two-way ANOVA). *C* the levels of *PRDX4* gene transcript is higher in patients with AR amplification than those without AR amplification. Data were obtained from the TCGA RNA-Seq data (*$p < 0.05$, unpaired Student's *t* test). *D* and *E*, amplification of *PRDX4* gene in prostate cancer patients correlates with shorter time in the duration of disease-free survival (*D*) and overall survival (*E*). Altered group in *red* indicates patients with *PRDX4* amplification; unaltered group in *blue* indicates patients without *PRDX4* amplification.

transcripts in tumors are all significantly higher than normal but there is no further increase as the cancer progresses (Fig. 1B). However, when transcript levels of *PRDX4* were compared between patients with or without androgen receptor (AR) amplification, there is a significant increase in samples with AR amplification (Fig. 1C), indicating that *PRDX4* may be activated by AR signaling. Furthermore, compared with those without, patients with *PRDX4* gene amplification has significantly shortened disease-free survival (Fig. 1D) and significantly reduced probability of overall survival (Fig. 1E).

### Screening for anti-Prx4 antibody that specifically recognizes Prx4 and antibody authentication

In order to identify an antibody that only recognizes Prx4, we obtained several commercially available anti-Prx4 antibodies and tested their potency and specificity using immunoblotting to detect endogenous Prx4 in various tissue/cell lysates from WT mice, Prx4 KO mice, or established human cell cultures. One antibody that specifically recognizes mouse or human Prx4 while has no cross-reaction with other proteins was obtained and used in this study. For example, Western blotting results indicated that this antibody recognizes both normal version of Prx4 in total lysates of various mouse organs and a spliced variant of Prx4 with higher molecular weight that only existed in the testis (27, 28) (Fig. S2A). The specificity of this antibody is also confirmed in lysates from mice with whole body KO of Prx4 since anti-Prx4 band is completely lost in Western blot except the testis-specific Prx4 as previously reported (28) (Fig. S2B). The specificity of this antibody to recognize

human Prx4 was also further validated and authenticated by the presence/absence of only one band in the following studies by comparing its expression in control and Prx4 knockdown or KO cell lines.

### Prx4 is highly expressed in prostate cancer patient specimens and cell lines derived from prostate cancer

To verify bioinformatic analysis results and to study the role of Prx4 in prostate cancer development, firstly we examined the levels of Prx4 protein in human prostate normal and cancer tissues by immunostaining using commercial tissue microarray slides. Samples include human prostate normal (n = 50) and adenocarcinoma (n = 66). As scored by the pathologist, we found that there is a significantly increased staining of Prx4 overall score in prostate adenocarcinoma compared with normal prostate. When further grouped by Gleason grade, there is no significantly increased score of Prx4 staining between different groups (Fig. 2C). Next, we examined the protein levels of Prx4 in various human prostate nontumorigenic or tumor cell lines. Cell lysates from a panel of prostate-derived cell lines including nontumorigenic (RWPE1), benign prostatic hyperplasia (BPH1), AR-positive adenocarcinoma (LNCaP, C4-2, and 22Rv1), and AR-negative adenocarcinoma (PC3 and DU145) were subjected to Western blotting. In all these cells, there is only band of anti-Prx4 detected with molecular weight around 27 KDa, which rules out the possibility of testis-specific Prx4 in these cells (Fig. 2D). Moreover, the levels of Prx4 in cell lines established from prostate tumors are significantly higher than those of the nontumorigenic RWPE1 cells (Fig. 2D bar graph).
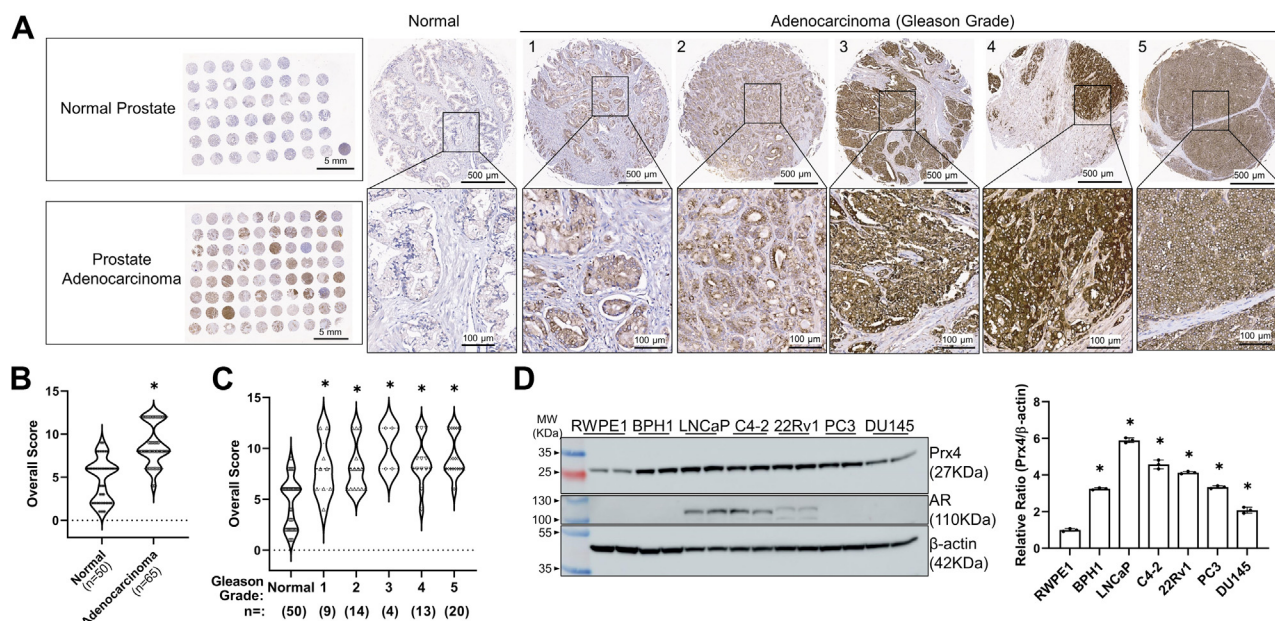


**Figure 2. Examination of Prx4 protein levels in patient specimens of prostate cancer by tissue microarray or established prostate cancer cell lines by Western blotting.** *A*, tissue microarray slides and representative images of anti-Prx4 staining of prostate normal and adenocarcinoma. Positive anti-Prx4 staining shows in *dark brown* and counter staining for nuclear shows *light blue*. The scale bars represent 5 mm (whole slide), 500 μm (individual tumor), and 100 μm (zoomed in). *B* and *C*, anti-Prx4 staining intensity were quantitatively scored by board-certified pathologist and data were compared between prostate normal (n = 50) and adenocarcinoma (n = 66) (*B*), as well as between prostate normal and cancer with different levels of Gleason grading (*C*). *D*, examination of Prx4 levels in prostate derived nontumorigenic or tumor cell lines by Western blotting. The bar graph on the right shows quantitative data from three independent blots. * $p < 0.05$ by two-way ANOVA. Prx, peroxiredoxin.

Taken together, these data suggest that the levels of Prx4 are highly expressed in patient specimens of prostate cancer and prostate tumor–derived cell lines.

### Prx4 is a downstream target of AR signaling activation

Interestingly, the levels of Prx4 in AR-positive cell lines (LNCaP, C4-2, and 22Rv1) show a trend of being higher than in cell lines without detectable levels of AR expression (Fig. 2D), raising the possibility that Prx4 may be positively regulated by the activation of AR signaling. To test this possibility, the PROMO platform was used to determine whether there are conserved androgen response elements (a 15 bp palindromic sequence containing two hexameric 5′-AGAACA-3′ half sites arranged as an inverted repeat with a 3 bp spacer) within the *PRDX4* gene promoter region (29, 30). From transcription start site of *PRDX4* to the upstream promoter of 5.1 Kbps, a total of seven putative AR-binding sites were identified (Table S1). To test whether these elements are involved in the regulation of Prx4 expression, cells were treated with R1881, a synthetic hormone that is known to bind AR leading to its translocation into the nucleus to bind and activate androgen response element–containing promoters. We found that treatment of LNCaP cells with R188 led to a robust, dose-dependent increased expression of Prx4, along with similar effect on the expression of PSA in these cells as expected (Fig. 3A). However, treatment of C4-2 or 22Rv1 failed to activate either the expression of Prx4 or PSA (Fig. 3A), for which reasons are unknown.

To further validate that Prx4 is activated by AR signaling in LNCaP cells, mouse xenografts through subcutaneous injection of LNCaP cells were generated. After tumor reached 100 mm$^3$, mice were separated into two groups receiving either sham surgery or castration, and tumor growth was monitored for 2 weeks before euthanasia. In consistence with similar studies from literature (31, 32), we found that castration led to significantly reduced rate of tumor growth as indicated by the comparison of tumor growth curve (Fig. 3B) and final tumor weight (Fig. 3C). Lysates from tumors were subjected to Western blotting to determine the levels of Prx4, PSA, AR, and β-actin, and we found that tumors from castrated mice have much lower PSA and Prx4 levels compared to tumors from control mice (Fig. 3D). These data indicate that sustained activation of AR signaling is required to maintain the high levels of Prx4 expression in LNCaP xenografts and to support its continued growth in mice.

### Depletion of Prx4 in prostate cancer cells delays cell cycle progression, inhibits cell migration, and invasion

To study the function of Prx4 in prostate cancer, lentiviral-mediated shRNA knockdown and CRISPR/Cas9-mediated KO techniques were used to generate cell lines that are depleted of endogenous Prx4. In both LNCaP and DU145 cell lines, compared with control cells expressing nontarget shRNA (shNT), stable expression of shRNA targeting the coding region of Prx4 (shPrx4) leads to the complete loss of endogenous Prx4 protein expression, whereas other proteins' expression such as Prx1 remains unaffected (Fig. 4A). The targeting specificity of shPrx4 has been described in previous study in our lab (14). To establish Prx4 KO cells using CRISPR-Cas9 technique, we designed two separate guide RNAs (gRNAs) targeting the *PRDX4* gene and their efficiency to KO endogenous Prx4 was compared as shown in the supplementary data (Fig. S3A). We found that gRNA1 had a higher KO efficiency than that of gRNA2. Therefore, gRNA1 was used to generate
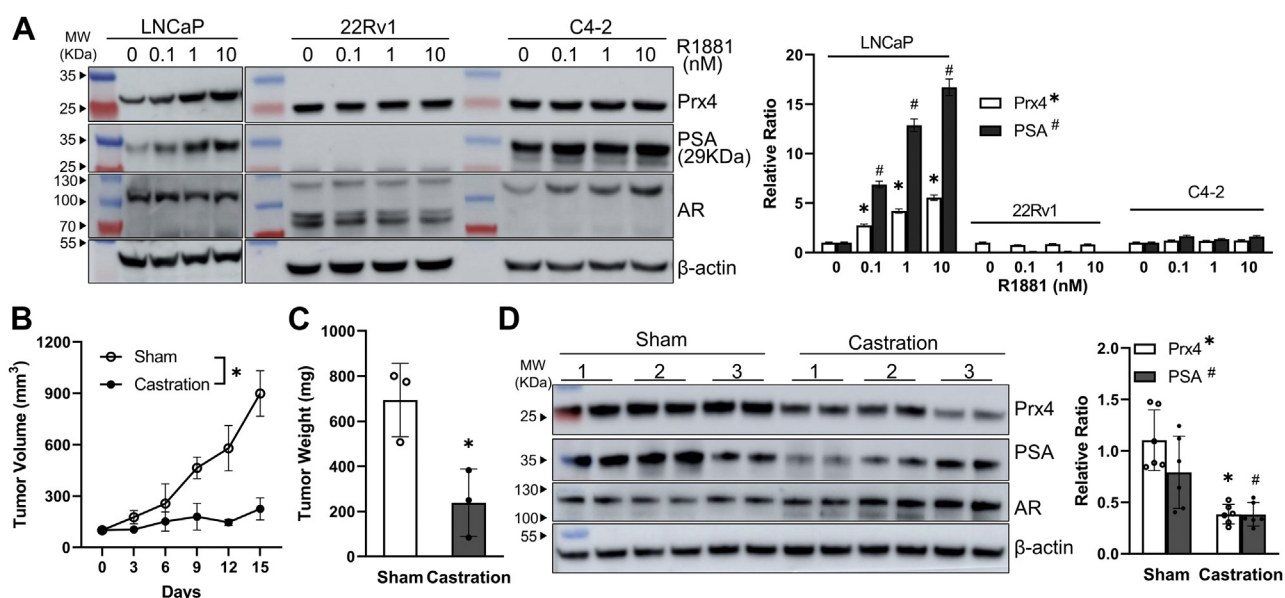


**Figure 3. The expression of Prx4 is activated by AR signaling in both cell culture and mouse models.** *A*, indicated cell lines were treated with or without increasing doses of R1881 to activate AR signaling. PSA is a known positive control of AR activation. The bar graph on the right shows quantitative data from three independent blots. *B*, tumor growth curve and final tumor weight (*C*) in mice receiving LNCaP cells without (Sham) or with surgically removal of both testicles (Castration). *D*, lysates from mouse xenograft tumors were subjected to Western blot to examine the levels of Prx4, PSA, and AR. Results of duplicates from each lysate of individually numbered mouse were shown. The bar graph on the right shows quantitative results of (*D*). In all bar graphs, * $p < 0.05$ (two-way ANOVA). AR, androgen receptor; Prx, peroxiredoxin; PSA, prostate-specific antigen.
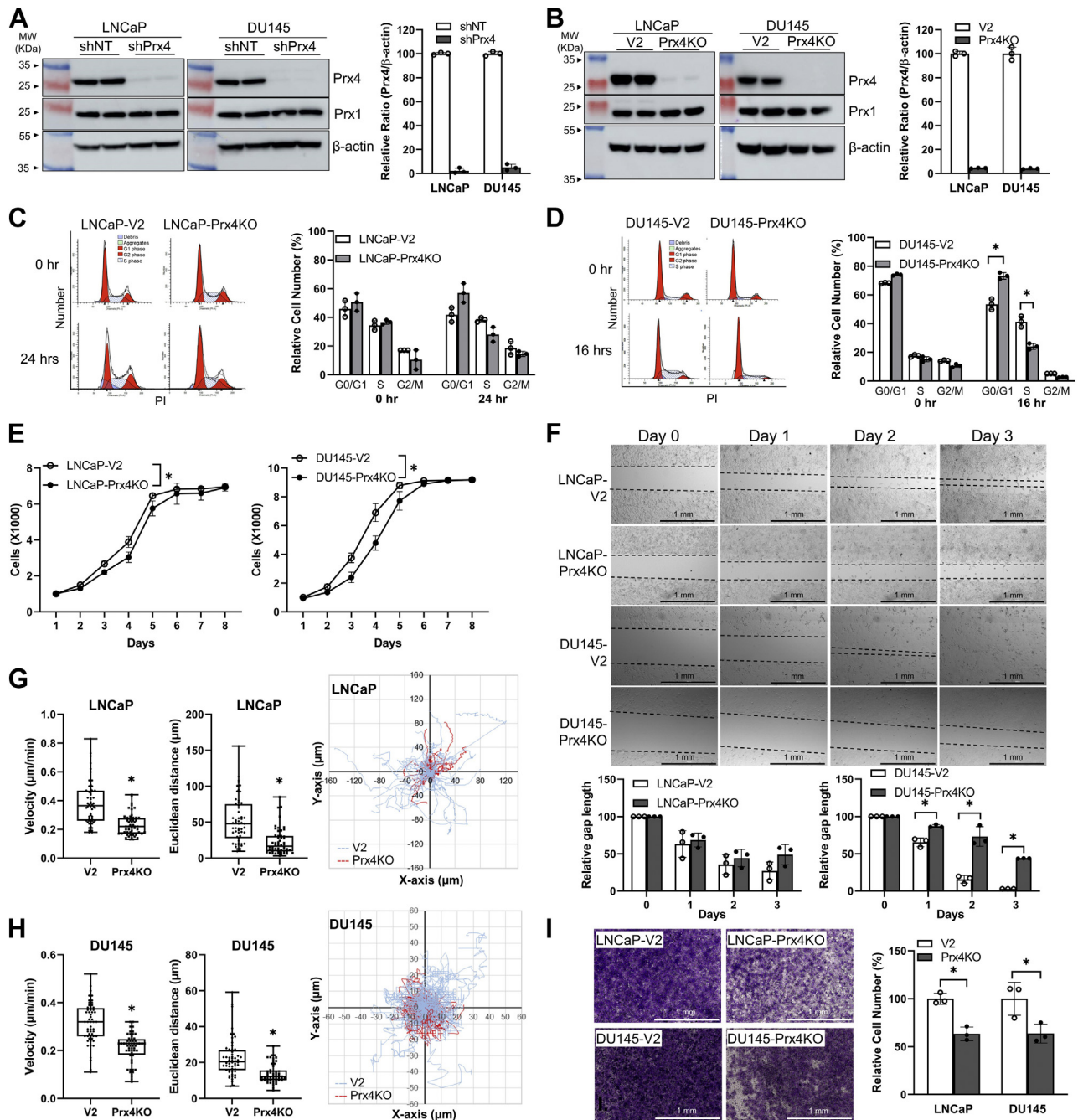
**Figure 4. Depletion of Prx4 in prostate cancer cell lines inhibits cell cycle progression, proliferation, migration, and invasion.** *A*, depletion of endogenous Prx4 in LNCaP and DU145 cell lines by stably expressing of shRNA targeting *PRDX4* coding region. Representative images of Western blots with duplicate samples are shown and quantitative results are shown on the right. *B*, depletion of endogenous Prx4 in LNCaP and DU145 cell lines using the CRISPR-Cas9 techniques and quantification are shown on the right. *C* and *D*, cell cycle analysis by flow cytometry. Cells cultured with serum starvation for 24 h and treated with serum-containing medium. After 16 or 24 h, the percentage of cell in G0/G1, S, and G2/M phased were determined using PI staining. The bar graph on the right shows quantitative results of triplicate samples. *E*, KO of Prx4 inhibits the cell proliferation. Same number of cells were seeded into 96-well plate and cell number is determined using CCK8 assay for consecutive 8 days. (*F*,) loss of Prx4 inhibits cell migration in wound healing assay. *p* < 0.05 by two-way ANOVA. *G* and *H*, cell movement tracking analysis using CellTracker software. Data (velocity and moving distance) in bar graph were obtained from more than 50 cells tracked in each group. Examples of cell moving routes were shown in the right panel. *I*, Matrigel invasion assay. Cells were seeded in plain medium in upper chamber and medium containing 10% FBS was added into bottom chamber as chemoattractant. Invaded cells were stained using crystal violet and quantitated with ImageJ software. The scale bars in (*F*) and (*I*) represent 1 mm. *In all graphs, compared with control, *p* < 0.05 (one-way ANOVA). FBS, fetal bovine serum; PI, propidium iodide; Prx, peroxiredoxin.

KO cells from both LNCaP and DU145 cell lines, and cells including LNCaP-Prx4KO8 and DU145-Prx4KO3 with complete loss of Prx4 were established and used in all following experiments (Fig. S3*B*). In addition to Western blotting,

immunostaining was used to further confirm that loss of Prx4 expression is true at individual cell level in both knock out cell lines (Fig. S3*C*). These data also confirm that anti-Prx4 antibody specifically recognizes Prx4. In both LNCaP and

DU145 cell lines, KO of Prx4 does not affect the expression of other Prxs such as Prx1 (Fig. 4*B*).

To study the effect of Prx4 depletion on cell growth and proliferation, firstly we used flow cytometry to evaluate the impact of depleting Prx4 on cell cycle progression. Cells were synchronized by serum starvation and cell cycle progression was reinitiated by the stimulation with serum containing medium. As shown in Figure 4*C*, there is a significantly greater number of Prx4-depleted LNCaP cells retained in the G0/G1-phase of cell cycle, while much fewer of these cells progressed into the S-phase. Similar results of fewer cells in S-phase were observed in Prx4 KO cells established from DU145 cell line (Fig. 4*D*). In both cell lines, the rate of cell proliferation as indicated by the calculation of doubling time in Prx4 KO cells is significantly reduced compared to those of control cells (Fig. 4*E*). Therefore, these data suggest that depletion of Prx4 in prostate cancer cells delays cell cycle progression and leads to the reduced rate of cell proliferation under adherent conditions.

To examine whether loss of Prx4 causes other phenotypic changes in prostate cancer cells, assays for cell migration and invasion were performed. To evaluate cell migration, wound-healing assays and cell movement tracking analysis were performed. Wounds in cultured cells were created by scratching. We found that KO of Prx4 in either LNCaP or DU145 cell lines leads to similar results of delayed closure of the wounded gap (Fig. 4*F*), indicating that Prx4 KO cells are less migrative than control cells. However, the interpretation of this result may be affected by the difference on the rate of cell proliferation. To solve this concern, time-lapse images of cells in culture were obtained and videos were generated. As shown in the video of cultured LNCaP cells as an example, control cells are highly migrative and constantly moving around, whereas Prx4 KO cells are much less active in movement (supplementary video v1 and v2). To quantify moving speed and distance, cell movement tracking analysis was performed using CellTracker software (http://www.celltracker.website/index. html) as previously reported (33). In both cell lines, we found that KO of Prx4 leads to significant decrease of moving velocity and distance (Fig. 4, *G* and *H*). Therefore, these data indicate that loss of Prx4 inhibits cell migration and movement. To study the effect of Prx4 loss on cell invasiveness, Matrigel invasion assays were performed, with equal number of control or Prx4 KO cells being seeded into invasion chambers. Cells invaded through Matrigel were stained and counted. We found that significantly low number of Prx4 KO cells were able to invade through Matrigel in both LNCaP and DU145 cell lines (Fig. 4*I*), indicating that Prx4 KO cells are less invasive. Taken together, these data suggest that loss of Prx4 leads to reduced rate of cell proliferation and inhibition of both cell migration and invasion.

### Prx4 contributes to the full activation of the Akt/GSK3α/β signaling

To further explore molecular mechanism by which Prx4 contributes to the growth, proliferation, migration, and invasiveness of prostate cancer cells, we used proteome profiler human phosphokinase arrays to examine the impact of Prx4 depletion on kinase signaling. On a single membrane preloaded with site-specific antiphosphorylation antibodies along with positive and negative controls, this array detects the activated levels of a total of 37 kinases in duplicate samples as listed in the supplementary data (Table S2). LNCaP control and Prx4 depleted cells were synchronized by serum starvation and then stimulated with serum-containing medium for 1 h, and cell lysates were harvested for the assay. Among all phosphorylated kinases examined, the levels of activated Akt and GSK3α/β are significantly reduced in Prx4 knockdown cells compared to those of control cells (Fig. 5*A*). To further confirm this observation, cells were starved overnight and replenished with complete culture medium–containing serum. Cell lysates were then collected at different time points after serum addition, and Western blotting was performed with site-specific antiphosphorylation antibodies. We found that there are lower levels of activated Akt and GSK3α/β in Prx4 knockdown cells, and similar trend was found in the activation of upstream kinase PDK (Fig. 5*B*). In addition, increased activity of PP2A in Prx4-depleted cells may also partially contribute to the decreased phosphorylation of AKT and/or GSK3α/β. Taken together, these data indicate that loss of Prx4 compromises the activation of kinase signaling including an insufficient activation of Akt and GSK3α/β signaling pathways.

### Depletion of Prx4 sensitizes prostate cancer cells to radiation through the inhibition of cells' ability to scavenge hydrogen peroxide and to recover from DNA damages

Radiation is commonly used as an effective strategy in the clinic to treat prostate cancer patients; we thus examined whether loss of Prx4 affects the efficacy of radiation treatment. Cells in culture were subjected to one-time, increasing doses of radiation. Ability of cell to survive and proliferate post-irradiation was evaluated by the comparison of $IC_{50}$ using clonogenic assay. As shown in Figure 6*A*, the $IC_{50}$ of radiation for LNCaP control cells is around 2.50 Gy, while the $IC_{50}$ of LNCaP-shPrx4 cells is only about 1.26 Gy, suggesting that shPrx4 cells are more sensitive to radiation. Similar results were found in DU145 cells, as the $IC_{50}$ of control cells is around 4.50 Gy, which is reduced to 3.40 Gy in Prx4 KO cells (Fig. 6*B*). These data suggest that depletion of Prx4 sensitizes prostate cancer cells to radiation.

To study molecular mechanism by which loss of Prx4 leads to cells' sensitization to radiation, firstly we asked whether depletion of Prx4 affects cells' ability to scavenge $H_2O_2$ since radiation leads to rapid generation of large amounts of ROS. Control and Prx4-depleted cells were treated with a short burst of increasing amounts of $H_2O_2$ to mimic radiation-induced acute oxidative stress, and the steady levels of ROS were measured using dichlorofluorescein-diacetate (DCF-DA)–based fluorescence method. In both LNCaP and DU145 cells, we found that depletion of Prx4 does not significantly affect basal/endogenous levels of ROS or impair their ability to scavenge low levels of exogenous $H_2O_2$
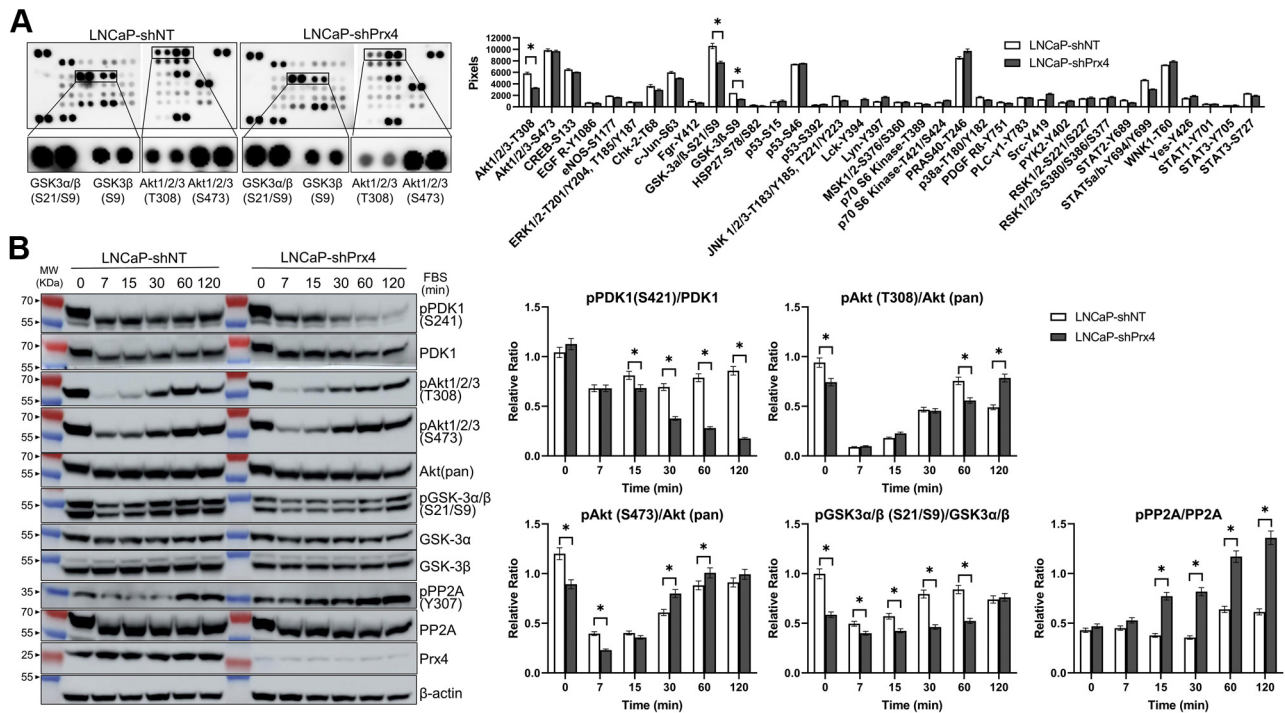
**Figure 5. Identification and validation of kinase signaling changes in Prx4-depleted cells.** *A*, proteome profiler human phosphokinase arrays using LNCaP-shNT and LNCaP-shPrx4 cell lysates. Framed spots indicated the levels of phosphorylated GSK3α/β and phosphorylated Akt in original (*top*) and zoomed in images (*bottom*). Bar graph on the right shows quantification results of duplicate samples. *B*, validation of findings in (*A*) by Western blotting. Cells were serum starved overnight and replenished with fresh medium for different time period, and cell lysates were collected for Western blotting. Quantification results were shown in right. *In all bar graphs, compared with control, $p < 0.05$ (one-way ANOVA). Prx, peroxiredoxin.

(Fig. 6*C*). However, when exposed to higher concentration of exogenous $H_2O_2$, the ability of Prx4-depleted cells to scavenge $H_2O_2$ is significantly reduced (Fig. 6*C*). In order to further consolidate these findings, a C-terminal Flag-tagged Prx4 (Prx4Flag) was introduced into LNCaP/DU145 KO cell lines, and levels of Prx4Flag in both cell lines were comparable to those of WT Prx4 in control cells (Fig. 6*D*). Upon radiation treatment, there is a significantly increased production of ROS in all cell lines, but Prx4-depleted cells have higher amounts of ROS accumulation after radiation, which is rescued by the expression of Prx4Flag (Fig. 6*E*). Therefore, depletion of Prx4 in prostate cancer cells impairs their ability to scavenge excessive ROS induced by radiation, which may contribute to their sensitization to radiation treatment.

Radiation leads to DNA double-strand breaks that have to be repaired for cells to survive. Next, we asked whether depletion of Prx4 in prostate cancer cells affect DNA damage response and cell apoptosis. In LNCaP cells, radiation leads to rapid stress response by accumulation of p53 in both control and Prx4 KO cells since these cells have WT *TP53* gene, whereas DU145 cells have abundant mutant p53 that does not change in response to radiation (Fig. 6*F*). In both cell types, radiation leads to robust DNA damages as indicated by the accumulation of γH2AX (Fig. 6*F*), a marker of DNA double-strand breaks. However, in both control cell lines, the levels of γH2AX decreases within a short time of 2 to 4 h, whereas the accumulation of γH2AX in KO cell lines continues to 8 to 24 h postirradiation, indicating either an increase of DNA damages or a decrease of their ability to repair. It is worth

mentioning that within 24 h of radiation treatment the trend in cell apoptosis as indicated by cleaved PARP and cleaved caspase 3 are similar between control and Prx4-depleted cells. To further confirm the difference in DNA damages between control and Prx4 KO cells, staining of γH2AX foci at 4 h postirradiation was visualized by fluorescent imaging, and we found that there are significantly more cells that are γH2AX positively stained, and restored expression of Prx4Flag rescues such defect (Fig. 6*G*). Therefore, these data suggest that depletion of Prx4 leads to sustained DNA damages in prostate cancer cells.

### Depletion of Prx4 leads to reduced tumor growth *in vivo and enhances the efficacy of radiation in mouse xenograft models*

To study whether the depletion of Prx4 in prostate cancer cells affects tumor growth *in vivo*, DU145 control and Prx4 KO cells were injected subcutaneously into the right flank of NOD SCID gamma male mice and tumor xenograft growth was monitored. As shown in tumor growth curve, the rate of tumor xenograft growth is much faster in mice injected with controls cells (Fig. 7*A*). After control group of mice reached to the euthanizing point, all mice were sacrificed and tumors were collected. We found that average tumor weight from mice injected with Prx4 KO cells is significantly lower than that of control group (Fig. 7*B*). LNCaP control and Prx4-depleted cells were also injected subcutaneously into the right flank of NOD SCID gamma male mice, and we found similar findings that loss of Prx4 reduces the rate of tumor xenograft growth
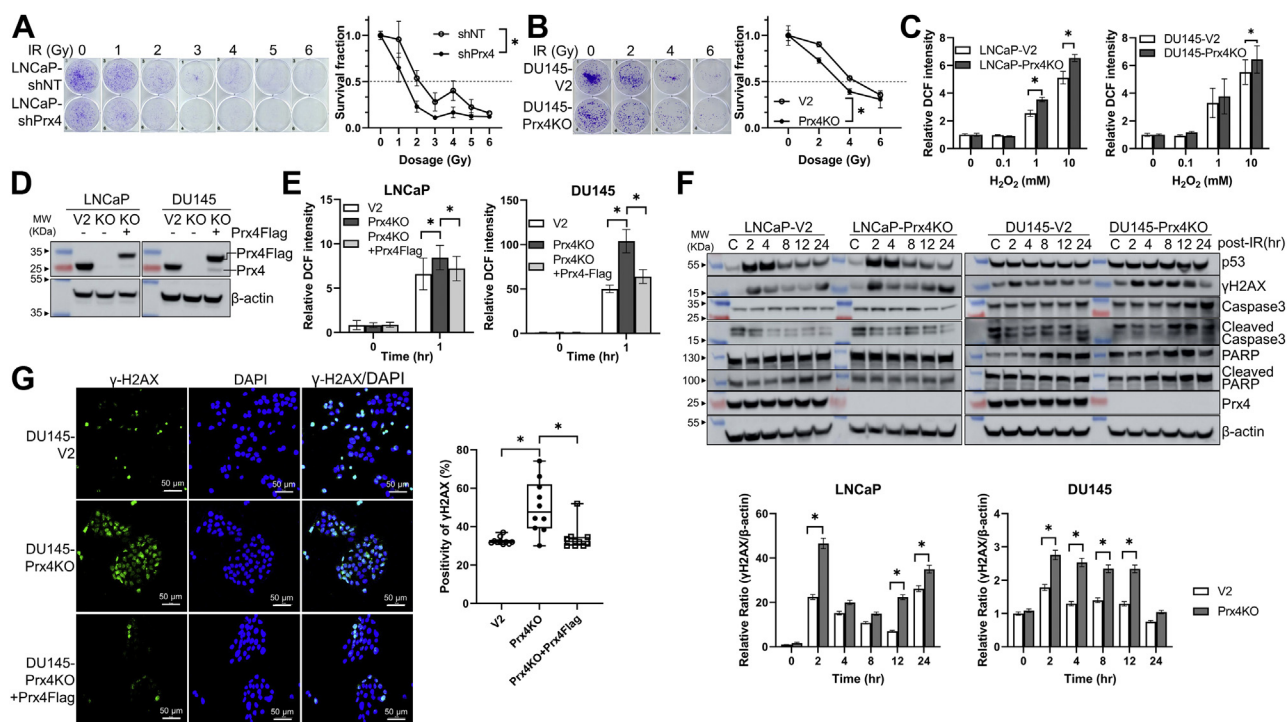
**Figure 6. Depletion of Prx4 sensitizes prostate cancer cell to radiation treatment.** *A* and *B*, cells were treated with increasing doses of ionizing radiation and then clonogenic assay was performed. Quantification results were shown on the right. *C*, cells were exposed to increasing concentration of $H_2O_2$ for 30 min and then rinsed with culture medium. Cells ability to scavenge $H_2O_2$ was then measured by using the DCF-DA assay. *D*, Western blotting shows the restoration of Prx4 expression in Prx4 KO cells with stably expression of Prx4Flag. *E*, indicated cell lines were subjected to one-time, 6 Gy of radiation, and levels of intracellular ROS were measured using the DCF-DA assay. *F*, indicated cell lines were subjected to one-time, 6 Gy of radiation, and cell lysates were harvested at indicated time points for Western blotting. Bar graphs on the bottom show quantitative results of γH2AX from LNCaP or DU145 cells. *G*, indicated cells were subjected to one-time, 6 Gy of radiation. At 4 hr postradiation, the levels of γH2AX were examined by immunofluorescence imaging (cells without radiation treatment did not show positive γH2AX staining). Quantification results were shown on the right. IR, irradiation. *Compared with control, $p < 0.05$ (one-way/two-way ANOVA). DFC-DA, dichlorofluorescein-diacetate; Prx, peroxiredoxin.

and final tumor weight (Fig. S4). Ki67 is marker of active cell proliferation, and the percentage of Ki67 positively stained cells in tumors from Prx4 KO cells is much lower than that of control (Fig. 7C), suggesting that the reduced tumor volume and weight of Prx4 KO tumors is due to the decrease of cell growth and proliferation. To further examine the effect of depleting Prx4 on the sensitivity of tumors to radiation *in vivo*, mouse xenograft tumors were first established by subcutaneous injection of control or Prx4 KO cells. In about 3 weeks, the average tumor volume reached 100 mm³ in both groups. Mice in both groups were then subjected to equal strength of tumor-localized radiation for three consecutive days for a total of 6 Gy. Mice were monitored for general health, and tumor growth was measured regularly. All mice were euthanized humanely at the same time when the control group of mice reached humanely health endpoint. As shown in Figure 8A, radiation leads to a temporary (about 3 weeks) pause of tumor growth in both groups. However, 3 weeks later tumors established from control cells were able to recover from radiation, and tumor volume continued to increase at a similar rate as observed in Figure 7A. In contrast, tumors established from Prx4 KO cells suffered from a prolonged effect of radiation with marginal gain of postradiation growth to the time point when mice in the control group have to be euthanized due to tumor burden. Compared with control group, the average weight of Prx4 KO tumors is also significantly lighter,

which is consistent with the reduced rate of tumor growth and smaller volume (Fig. 8B). Moreover, histology confirms that there are more tissue damages caused by radiation and fewer cells are positively stained with Ki67 in tumors of Prx4 KO cells compared to those of tumors from control cells (Fig. 8C). Taken together, these data indicate that loss of Prx4 inhibits tumor xenograft growth and sensitizes tumors to radiation in mouse models.

In summary, firstly we used meta-analysis to reveal that *PRDX4* gene is amplified and its transcripts are highly present in prostate cancer. At the protein level using authenticated anti-Prx4 antibody, we found that Prx4 is strongly present in patient specimens of prostate cancer and also highly expressed in cell lines derived from prostate tumors. Using two different prostate cancer cell lines and two independent strategies of depleting endogenously expressed protein, we demonstrated that loss of Prx4 delays cell cycle progression, inhibits cell migration and invasion, and sensitizes cells to radiation. Mechanistically, we demonstrated that Prx4 contributes to the activation of Akt/GSK3 signaling pathways in prostate cancer. Depletion of Prx4 also leads to a significant decrease of tumor xenograft growth *in vivo* and enhances the efficacy of radiation therapy in mouse models. Based on these findings, a model of how Prx4 contributes to prostate cancer development and radioresistance was proposed (Fig. 9). Our study also indicates that targeting Prx4 may be utilized as a potential strategy to
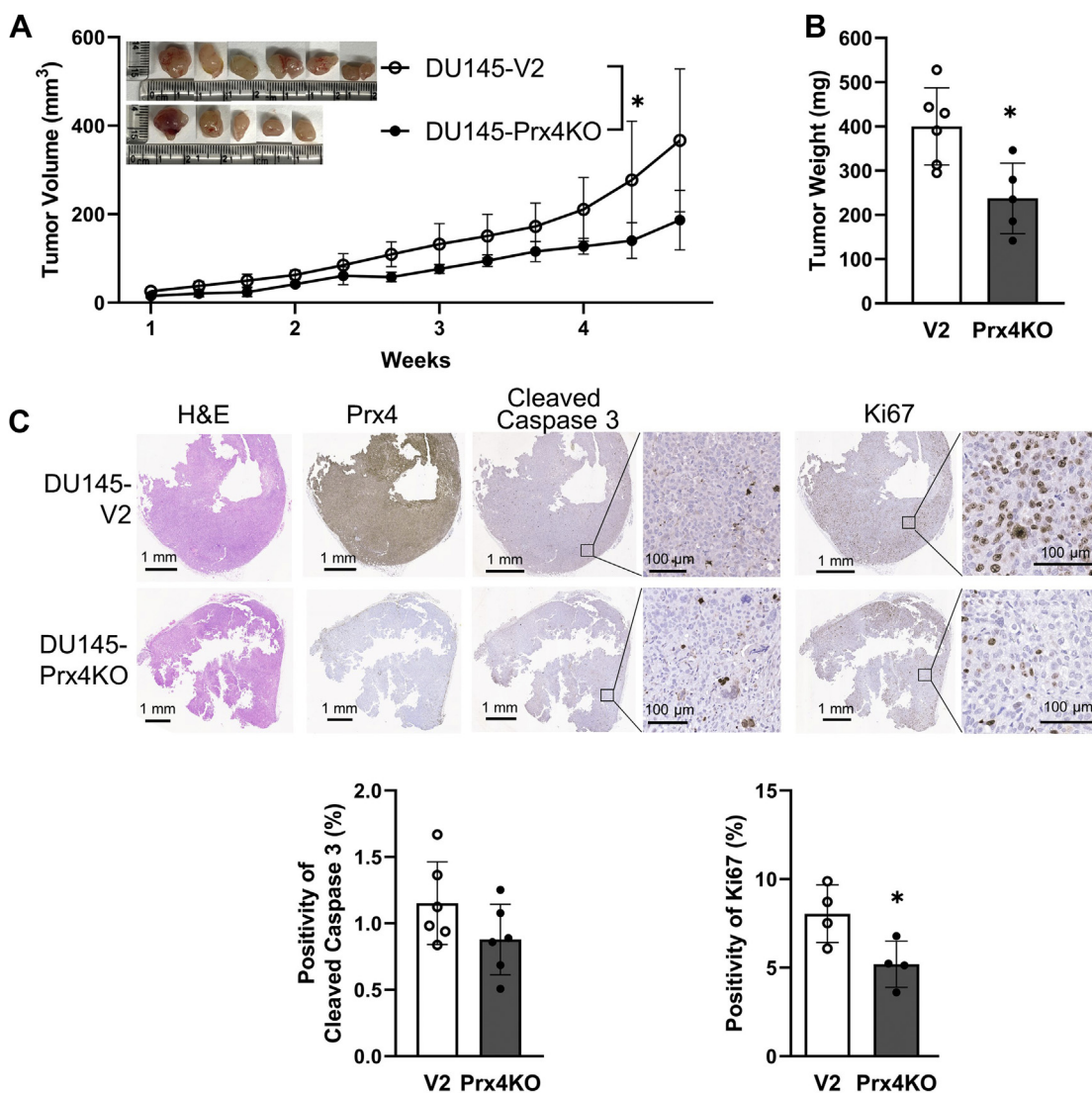
**Figure 7. Depletion of Prx4 significantly attenuates tumor growth in mouse xenograft model.** *A*, tumor growth curve. NSG-SCID mice were subcutaneously injected with either control (DU145-V2, n = 6) or Prx4-depleted cells (DU145-Prx4KO, n = 5). *B*, comparison of final tumor weight. *C*, histological comparison using H&E, anti-Prx4, anti-cleaved caspase 3, and anti-Ki67 staining of tumor sections. The scale bars represent 1 mm (tumor) or 100 μm (zoomed in). In all graphs, * $p < 0.05$ (*t* test). Prx, peroxiredoxin.

inhibit tumor growth or overcome the radioresistance of prostate cancer in patients.

## Discussion

The development of prostate cancer is strongly correlated with oxidative stress and aging (34). Oxidative stress is known to influence the activities of inflammatory mediators and other cellular processes involved in the initiation, promotion, and progression of human prostate cancer (35). Since cancer cells exhibit aberrant metabolism to satisfy needs of energy for rapid cell proliferation, they also generate high levels of ROS, which stimulates the expression of cellular antioxidants through the regulation of redox-sensitive transcription factors (36). Among those antioxidants, Prxs are the highly conserved and mostly abundant family of peroxidases that scavenge hydrogen peroxide as well as mediate redox signaling under both physiological and pathological conditions. It is well documented that the levels of most Prxs, such as Prx1, are upregulated and positively associated with poor prognosis in patients in various types of human cancer, including lung (37), breast (38), colon (14) and prostate cancer (16). However, whether and how the expression of Prxs contributes to cancer development and therapeutic resistance has not been completely explored.

In this study, firstly we identified that *PRDX4* gene is amplified in human prostate cancer, and prostate cancer patients with high levels of Prx4 have poorer survival through bioinformatic analysis of existing datasets. Aberrantly, high expression of Prx4 is confirmed in tumor specimens of prostate cancer patients and established prostate cancer cell lines. Interestingly, we found the Prx4 levels are higher in AR-positive prostate cancer cells (LNCaP, C4-2, and 22Rv1) than AR-negative cells (PC3 and DU145), indicating that Prx4 may be a downstream target of AR signaling activation. Indeed, seven potential AR-binding motifs are present in the *PRDX4*
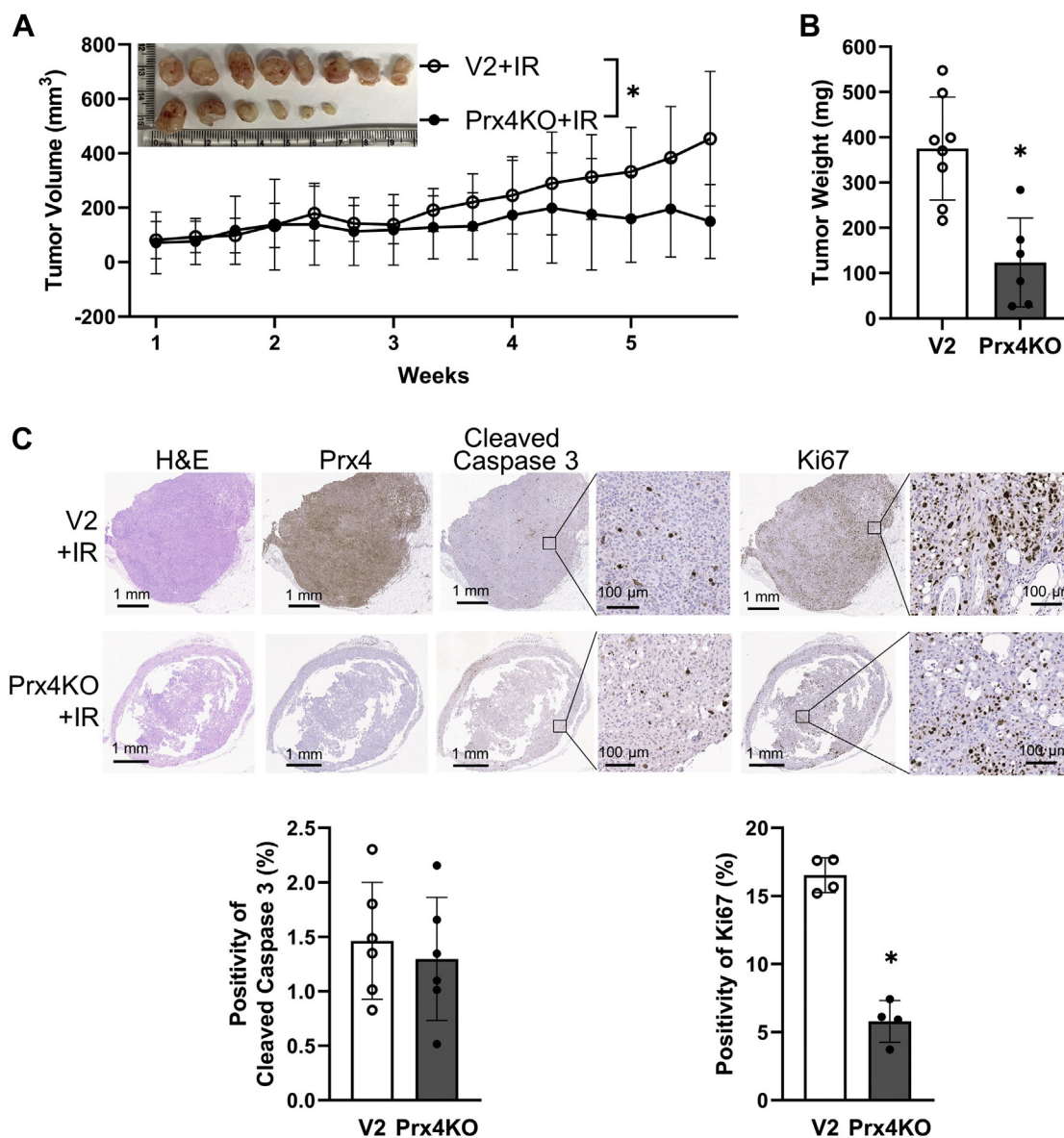
**Figure 8. Depletion of Prx4 sensitizes mouse xenograft to ionizing radiation.** *A*, tumor growth curve postradiation. NSG-SCID mice were subcutaneously injected with either control (DU145-V2, n = 8) or Prx4-depleted cells (DU145-Prx4KO, n = 6). After average volume of tumors reaches 100 mm$^3$ in each group, tumors were treated with 2 Gy of ionizing radiation once every day for 3 days. *B*, comparison of final tumor weight. *C*, comparison of tumors using H&E, anti-Prx4, anti-cleaved caspase 3, and anti-Ki67. The scale bars represent 1 mm (tumor) or 100 μm (zoomed in). In all graphs, IR: irradiation. * $p < 0.05$ (*t* test). Prx, peroxiredoxin.

gene promoter, and activation of AR-mediated pathway leads to robust stimulation of Prx4 in LNCaP cells. However, such stimulation of Prx4 expression was only observed in LNCaP cells, which are castration sensitive. In castration-resistant prostate cancer cell, including C4-2 and 22Rv1 cells, androgen-dependent stimulation of Prx4 was not prominently observed. This may partially be due to the intrinsic features of castration-resistant prostate cancer cells, including but not limited to, their hyperactive AR signaling in the absence of androgen (39), already contributing to high levels of Prx4 presence. However, the fact that the levels of Prx4 in AR-negative prostate cancer cells is still higher than those of nontumorigenic cells indicates that other mechanisms of regulation may also contribute to the increased expression

of Prx4, such as chromosomal rearrangement, DNA methylation, NF-κB, and Nrf2 signaling, etc. To fully understand the regulatory mechanism, it will be of interest to investigate whether and how these factors coordinate with AR signaling to control the levels of Prx4 in prostate or other cancer cells.

To study how increased expression of Prx4 contributes to prostate cancer development and therapeutic resistance, endogenously expressed Prx4 in two different prostate cancer cell lines were depleted using distinctive strategies including shRNA knockdown and CRISPR-Cas9 KO. The principle of lentiviral-based shRNA knockdown is that sequence-specific shRNA binds to the target mRNA leading to its degradation, whereas CRISPR-Cas9 utilizes single guide RNAs to edit target genes at the genomic DNA level, and KO is often achieved by
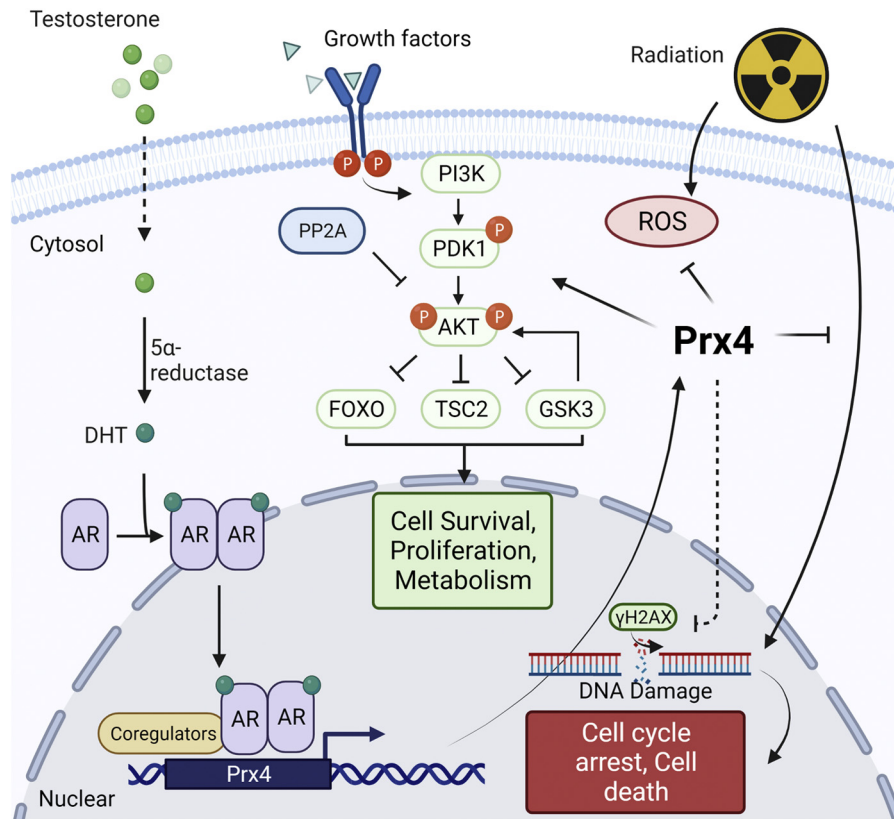
**Figure 9. A schematic model of Prx4 in prostate cancer malignancy and radiation resistance.** Prx, peroxiredoxin.

creating a premature stop codon in the target gene. Such application of both strategies to deplete Prx4 in this study can minimize the off-target effect of gene manipulation and reveal truly unbiased phenotypic changes that are associated with the loss of Prx4 protein in prostate cancer cells. With such combinational strategies, we demonstrated that loss of Prx4 leads to delayed cell cycle progression, reduced cell growth and proliferation, inhibition of cells' ability to migrate and invade through the Matrigel under standard cell culture conditions. To study the molecular mechanism by which Prx4 contributes to prostate cancer cell proliferation, migration, and invasion, proteome profiler phosphokinase array was used to compare the differences on kinase signaling between control and Prx4-depleted cells. We demonstrated that depletion of Prx4 leads to a profound change of kinase profiling including the insufficient activation of phospho-Akt, Chk-2, c-Jun, GSK3, JNK, Stat5, etc. We further investigated these signaling changes by focusing on the impact of Prx4 on the phosphorylation and activation of Akt pathway, since all other kinase changes can be the result of Akt signaling. The canonical pathway of AKT activation is initiated by the activation of receptor tyrosine kinases or G-protein-coupled receptors (GPCR) and subsequent recruitment and activation of one or more members of the PI3K family (40). Two major phosphorylation sites are critically involved in the regulation of AKT activation. Among them, T308 is located within the activation or T-loop of the catalytic domain, whereas S473 is located in the C-terminal hydrophobic motif (41). For the Akt to be fully activated, T308 has to be phosphorylated usually by the upstream

phosphoinositide-dependent protein kinase 1(PDK1) (42, 43); and S473 has to be phosphorylated, which can be carried out by the mechanistic target of rapamycin complex 2 (mTORC2) (44). Phosphorylation of both sites leads to the stabilization and activation of AKT to the full status (45). We found that the phosphorylation levels of AKT at both T308 and S473 sites in Prx4-depleted cells are less than that of control cells, indicating that loss of Prx4 compromises the full activation of AKT signaling. Indeed, this is further substantiated by the insufficient phosphorylation of Akt downstream mediators such as GSK3α/β. Under basal or starvation conditions, GSK3α/β is less active through Akt-mediated S9/21 phosphorylation, whereas such phosphorylation is inhibited in response to serum or growth factor stimulation (46). The dephosphorylated of GSK3α/β (S9/21) causes a structural conformation change by opening the catalytic site to its substrates, such as β-catenin, which is then phosphorylated and targeted for ubiquitination and degradation (47). Collectively, phosphorylation changes of these signaling molecules may cause secondary or even tertiary modification of intracellular signal transduction, leading to the observed effect of Prx4 depletion on prostate cancer cells.

In addition to the inhibition of cell proliferation and invasion, we found that prostate cancer cells depleted of Prx4 are much more sensitive to radiation. Besides changes on aforementioned kinase signaling, loss of Prx4 also compromises cells' ability to scavenge exogenously added or radiation-induced ROS, which is accompanied with increased accumulation of DNA damages after radiation. In mouse xenograft

models, we found that depletion of Prx4 leads to reduced tumor xenograft growth in immunodeficient mice, and tumors established by Prx4-depleted cells are much more sensitive to radiation treatment. Histological examinations revealed that tumors from Prx4-depleted cells are less proliferative, consisting with the finding from cell culture. In the clinic, patients with prostate cancer are often diagnosed early with only local or regional tumors, and their 5 year survival rate is close to 100% with proper treatment of radical prostatectomy, radiation, or the combination (6). Nevertheless, therapeutic ineffectiveness including radiation resistance is frequently developed in prostate cancer patients. Our finding that Prx4 depleted cells are more sensitive to radiation treatment both *in vitro* and *in vivo* indicate that high levels of Prx4 protect cells from radiation-induced damages and thus may facilitate cancer relapse and reoccurrence in patients. Therefore, future strategies of inactivating Prx4 by small molecules or gene editing may have potential value to increase the efficacy of radiotherapy and improve the prognosis of patients with prostate cancer.

In addition to our study, previously published studies also reveal that Prxs play a critical role in cancer cell invasion and metastasis. For example, Prx1 promotes colorectal cancer metastasis and angiogenesis by increasing the expression of MMP2, MMP9, and VEGF (48); Prx2 contributes breast cancer cell colonization in the lungs through the regulation on oxidative and metabolic stress response (49). Although whether and how Prx4 contributes to prostate cancer metastasis was not studied, our demonstration of Prx4 affected signaling changes in prostate cancer cells may shed light on the understanding of cellular antioxidant enzymes on cancer cell invasion and metastasis. However, due to the limited scope of the current study and resources, we were not able to investigate how the presence/absence of Prx4 contributes to prostate cancer metastasis in mouse models. Moreover, whether and how signaling changes observed in Prx4-depleted cells contribute to cancer metastasis and radiation resistance needs to be further studied.

## Experimental procedures

### Bioinformatic tools for meta-analysis and prediction of putative transcription binding sites

Meta-analysis was carried out using publicly or commercially available bioinformatic platforms including the Genomic Data Commons Data Portal at National Cancer Institute (https://portal.gdc.cancer.gov/), the cBioPortal for Cancer Genomics developed at Memorial Sloan Kettering Cancer Center (https://cbioportal.org/), the University of Alabama at Birmingham Cancer (UALCAN) data analysis portal (http://ualcan.path.uab.edu/index.html) (50), and Shiny Methylation Analysis Resource Tool (SMART) App (http://www.bioinfo-zs.com/smartapp/) (51). These platforms use multiple sources of datasets from The Cancer Genome Atlas (TCGA) or published literature that contain data of DNA/RNA sequencing, DNA methylation, transcript counting, and microarray results from variety of patient specimens. Prediction of transcription

factor–binding sites in the *PRDX4* gene promoter was performed using the PROMO virtual library platform (http://alggen.lsi.upc.es/) (52).

### Tissue microarray and immunostaining

Human prostate normal and prostate cancer tissue microarray slides were commercially obtained, including BNS19011 and PR803d (US Biomax). Tissue slides were rehydrated in xylene, and antigen retrieval was processed in the buffer containing target retrieval solution, citrate pH 6.0 (catalog no. S236984-2; Dako), 90% glycerol, and 1 mM EDTA. The immunohistochemistry staining was carried out using the VECTASTAIN ABC Kits (HRP) following the manufacturer's suggested protocol (PK-6200; Vector laboratories). The following primary antibodies were used for immunohistochemistry: Prx4 (1:500 dilution) (ab184167; Abcam), Ki67 (1:40 dilution) (ab16667; Abcam), and cleaved caspase 3 (1:50 dilution) (9661; Cell signaling technology). After counter staining with hematoxylin, positive staining appears to be dark brown in color as 3,3′-diaminobenzidine was used as the chromogen. Based on staining intensity, every specimen was given an intensity score by the board-certified pathologist as the following: completely negative (0), weakly positive (+1), positive (+2), and strongly positive (+3); every specimen was also given a staining quantity score based on the percentage of positive-staining cells as the following: no positively stained cells (0), 1% to 25% positive (1), 26% to 50% positive (2), 51% to 75% positive (3) and 76% to 100% positive (4). Overall score of each sample was thus obtained by intensity score × quantity score as previously reported (17). The slide was also visualized and analyzed using ImageScope software (version 11.2.0. from Aperio Technologies). For immunocytochemistry, cells were seeded onto poly-L-lysine–coated glass coverslip and cultured for at least 24 h before being fixed with 4% paraformaldehyde. After fixation, cells were washed with PBS once and blocked with 5% goat serum. After another blocking with 3% $H_2O_2$ for 10 min, cells were incubated with anti-Prx4 diluted in 1% bovine serum albumin (1:500) at 4 °C in a humidified chamber overnight. Cells were washed with PBS three times and incubated with horseradish peroxidase–conjugated secondary antibody for 1 h at room temperature (RT). 3,3′-Diaminobenzidine was used as the substrate, and slides were counterstained with hematoxylin (H-3404, Vector laboratories) and mounted with DPX Mountant (06522; Sigma–Aldrich). Staining images were taken using the Bio-Tek Cytation 5 image station (Agilent).

### Cell lines and reagents

RWPE-1, LNCaP, C4-2, 22Rv1, PC3, DU145, and HEK293T cell lines were originally purchased from American Type Culture Collection and cultured under recommended conditions including 100% humidified atmosphere with 5% $CO_2$ at 37 °C. Dulbecco's modified Eagle's medium (Gibco) supplemented with 10% fetal bovine serum (FBS) (Gibco) was used to culture HEK293T and DU145 cells. RPMI1640 medium (Gibco) supplemented with 10% FBS was used to culture

LNCaP, C4-2, 22Rv1, and PC3 cells. Keratinocyte-SFM medium (Gibco) was used to culture RWPE-1 cells. Penicillin–streptomycin solution (Hyclone) (where penicillin is 100 units/ml and streptomycin 100 μg/ml) and 5 μg/ml gentamicin (Gibco) were added to the medium before use. Puromycin (Gibco), 1 μg/ml, was added to establish stable cell lines infected with lentiviral shRNAs or pLentiCRISPR-V2.

### AR activation assay

For *in vitro* study, LNCaP, C4-2, and 22Rv1 were grown to 70% confluence in charcoal-stripped FBS (A3382101; Gibco) for 2 days before R1881 treatment (50152311; Thermo Fisher Scientific). Cells were treated with R1881 (0.1, 1, and 10 nM) for another 24 h in charcoal-stripped FBS before being harvested for immunoblotting.

### Establishment of stable knockdown/KO cells

To make stable knockdown cells, MISSION NonTarget shRNA (shNT) and shRNAs specifically targeting Prx4 (shPrx4) were commercially obtained and knockdown efficiency was screened as previously published (14). To establish Prx4 KO cell lines using CRISPR-Cas9 technique, gRNAs targeting for *PRDX4* gene (gRNA1: 5′-ACCTAAGCAAAGC GAAGAGT-3′, gRNA2: 5′-TACCCCAAAAGCCGCAGCTG-3′) were synthesized by Thermo Fisher Scientific. Annealed oligos were inserted into BsmbI site of the plasmid pLentiCRISPR-V2, which is a gift from Dr Feng Zhang's lab (52961; Addgene plasmid) (53). Lentiviral particles were generated following instruction in the manual using commercial packaging plasmid mix (SHP001; Sigma–Aldrich) and Lipofectamine 3000 transfection reagent (L3000001; Thermo Fisher Scientific) in HEK293T cells. Stable cells were established and maintained in 1 μg/ml puromycin-containing medium.

### Cell proliferation assay

Cells were seeded in 96-well plates at 1000 cells/well and incubated in a 100% humidified atmosphere with 5% $CO_2$ at 37 °C. Cell proliferation was assessed using the CCK-8 cell proliferation assay kit following the manufacturer's protocol (K1018; APExBIO). Briefly, 10 μl of CCK-8 reagent was added to each well and the plates were returned to the incubator for another 2 h. Absorbance was measured at 450 nm in a multiplate reader (GloMax-Multi Detection System, Promega). Tests were generated for consecutive 8 days.

### Clonogenic assay

Clonogenic assay was performed as previously published (54). Briefly, cells were seeded onto 6-well plates at 4000 cells/well. X-RAD 225XL (Precision X-ray) was used to perform irradiation at the dosage ranging from 1 to 6 Gy. After irradiation, cells were incubated in a 100% humidified atmosphere with 5% $CO_2$ at 37 °C for about 3 weeks. Cells were then fixed with 4% formaldehyde for 15 min, stained with 0.5% (w/v) crystal violet for 30 min, then gently rinsed with tap water.

Staining images were taken by scanner and ImageJ (https://imagej.nih.gov/ij/download.html) was used to quantify the number of colonies.

### Cell cycle analysis

Cells were seeded in 100 mm dishes to reach 70% confluency. They were synchronized by serum starvation for 24 h and restored to culture in complete medium containing 10% FBS. Cells were then collected at 0, 16, and 24 h by trypsinization. Cell cycle assay was performed following a well-established protocol (55). Briefly, cells were washed in PBS twice and fixed in 70% ice-cold ethanol at −20 °C for 24 h. For propidium iodide (PI) staining, cells were washed with ice-cold PBS twice and then resuspended in 500 μl PI/Triton X-100 staining solution (10 ml of 0.1 % Triton X-100 in PBS with 2 mg of DNase-free RNase A and 0.40 ml of 500 μg/ml PI) and incubated for 30 min at RT. Staining was then visualized by Cytometers BD LSR II and data were analyzed using ModFit LT software (BD Bioscience; https://www.bdbiosciences.com/).

### Cell migration analysis

Cell migration was evaluated using wound-healing assay and cell movement tracking analysis. For wound healing, cells were seeded in 12-well plate and cultured for 24 h before scratching with a p200 pipet tips following a well-established protocol (56). Images were captured using BioTek Cytation 5 every 24 h until the control group filled the gap. Results were quantified with ImageJ software. For cell movement tracking, cells were seeded onto collagen-coated chamber slide and cultured for 16 h, and time-lapse videos were captured using BioTek Cytation 5 at 10 min per frame for a duration of 10 hours. CellTracker software was used to quantitate the movement of cells as previously reported (33). Average speed of movement for each cell was calculated as the sum length of the cell's trajectory divided by the total time over which the trajectory was measured. To compare average speed and maximum distance from origin of each group, data from at least 50 cells were collected, and the Kruskal–Wallis test was used examine statistical significance.

### Cell invasion assay

Matrigel 50 μl/well at 100 μg/ml was added to a 24-well *trans*-well insert and solidified in a 37 °C incubator for 30 min to form a thin layer of invasion matrix. About $1 \times 10^5$ cells in plain medium were seeded into the pretreated *trans*-well insert, and 600 μl complete culture medium was added to the bottom chamber. Cells were cultured in a 100% humidified atmosphere with 5% $CO_2$ at 37 °C for 2 days. The Matrigel layer was then removed, and cells invaded through Matrigel onto the other side of the membrane were stained with 0.5% (w/v) crystal violet (57). Microscopic images were taken using BioTek Cytation

5. The number of invaded cells was quantitated using ImageJ software.

## Measurements of intracellular ROS

Levels of intracellular ROS were detected using DCF-DA−based method (58). Briefly, cells were plated at a density $4 \times 10^4$ cells/well in 96-well plate for 24 h. Cells were then treated with or without $H_2O_2$ for 30 min at 0.1, 1, 10 mM, washed with PBS for three times, and stained with DCF-DA (25 μM) for 45 min at 37 °C, and fluorescence intensity was determined using BioTek Cytation 5. For radiation-induced ROS measurements, $4 \times 10^4$ cells/well were seeded into 96-well plates and allowed to attach overnight. Cells were irradiated at 6 Gy, and DCF-DA fluorescence intensity was recorded before and 1 h after radiation.

## Immunocytochemistry for γH2AX

About $1 \times 10^5$ cells were seeded into 8-well chamber slice for 24 h. Cells were fixed by 4% paraformaldehyde 4 h after exposing to 6 Gy radiation. Cells were then permeabilized with 0.1% Triton-X 100 in PBS for 10 min at RT. After permeabilization, cells were washed with PBS for three times (10 min for each time) and blocked with 5% goat serum in PBS for 1 h at RT. Then, cells were washed with PBS for three times and incubated with rabbit mAb against Phospho-Histone H2AX (serine 139) (1:100 dilution) (AP0687; ABclonal) for overnight at 4 °C. After incubation, cells were washed with PBS for three times and stained with F(ab')2-Goat anti-rabbit IgG (H + L) cross-adsorbed secondary antibody, Alexa Fluor 488 (1:1000) (A-11070; Invitrogen) in PBS for 1 h at RT. Then, cells were washed with PBS for three times and mounted with ProLong Gold Antifade Mountant with 4′,6-diamidino-2-phenylindole (P36935; Thermo Fisher Scientific). The fluorescence images were captured using Nikon A1Rsi confocal microscope.

## Western blotting

Cells were cultured in 100 mm dishes or 6-well plate and harvested in radioimmunoprecipitation assay lysis buffer (sc-24948; Santa Cruz Biotechnology). Proteins were separated on SurePAGE (M00654; GenScript) gel by electrophoresis and transferred to polyvinylidene difluoride membrane. Membranes were blocked for 1 h in 5% nonfat dry milk in Tris-buffered saline (TBS) before overnight incubation with diluted primary antibody. The membrane was then washed with TBS and incubated for 1 h with either rabbit or mouse IgG horseradish peroxidase−conjugated secondary antibody (R&D systems). After multiple washing steps, the signal was detected using Amersham ECL Select Western Blotting Detection Reagent and bands were visualized by Amersham Imager 680 (GE healthcare). Primary antibodies used in this article include anti-Prx4 (ab184167; Abcam, 1:10,000) and anti-β-actin (A2228; Sigma−Aldrich, 1: 5000). Antibodies for phosphorylated GSK3α/β (S9/S21), total GSK3α/β, phosphorylated Akt (T308), phosphorylated Akt (S473), Akt (total),

phosphorylated PDK, total PDK (S241), phosphorylated PP2A (Y307), PP2A, cleaved caspase 3, and caspase 3 (total) were from Cell Signaling Technology using 1:1000 dilution.

## Mouse xenograft experiments

All mouse procedures were reviewed and approved by the University of Kentucky IACUC review board (protocol #2016-2306). The NOD.Cg-Prkdcscid Il2rgtm1Wjl/SzJ mice were purchased from the Jackson Laboratory and housed under specific pathogen-free conditions in individual-ventilated cages in a 12 h light−dark cycle and were provided with a standard rodent diet and water *ad libitum*. To study the AR signaling *in vivo*, $1.5 \times 10^6$ LNCaP cells mixed with Matrigel (1:1) were subcutaneously injected to 8-week-old male mice. Tumor growth was monitored by measuring orthogonal diameters of tumors once every other day with a digital caliper. The tumor volume, V, was calculated with the formula $V = (lw^2/2)$, where $l$ is the longest axis of the tumor and $w$ is the axis perpendicular to $l$. When the tumor volume reached 100 mm³, mice were randomly separated into two groups, one control with intact male reproductive system and one castration group by removing both testes. Two weeks after castration, both control group and castration group mice were euthanized and tumors were collected. Prx4 expression levels were examined by Western blot. To study tumor growth, $2 \times 10^5$ DU145-V2 or DU145-Prx4KO cells or $1.0 \times 10^6$ LNCaP-V2 or LNCaP-Prx4KO cells, were mixed with Matrigel (1:1 in volume) and subcutaneously injected to 6-week-old male mice. Tumor growth was monitored till euthanasia point (when the longest axis of control tumor reached to 10 mm). To study radioresistance of mouse xenografts, $2 \times 10^5$ DU145-V2 or DU145-Prx4KO cells were subcutaneously injected to 6-week-old male mice. When the average tumor volume reached 100 mm³, mice were subjected to tumor-localized irradiation with 2 Gy for three consecutive days using X-RAD 225XL (Precision X-ray). After radiation, tumor growth was monitored, and mice were euthanized when the longest axis reached to 10 mm. Data were analyzed using GraphPad Prism 9 software (GraphPad Software).

## Phosphokinase profiling assay

Cells were cultured in 100 mm dishes to reach 90% confluency. Then, cells were synchronized by serum starvation for 24 h and restored to complete medium with 10% FBS for another 1 h. Cell lysates were harvested using 1 ml radio-immunoprecipitation assay buffer. Protein assay was performed using *DC* protein assay kit (5000111; Bio-Rad). Protein phosphorylation assays were performed following the user manual of Human Phospho-Kinase Array kit (R&D). ImageJ and GraphPad Prism 9 were used to quantitate and analyze data, respectively.

## Statistical analysis

GraphPad Prism 9 software was used for statistical analyses and visualization. Normally distributed data is analyzed for

significant group differences using a two-tailed unpaired Student's *t* test. Nonparametric Mann–Whitney *t* test (two-tailed) is used for non-normally distributed data. For repeated measures over time, two-way ANOVA and Bonferroni post-test are performed. $p < 0.05$ is considered statistically significant (*$p < 0.05$). All Western blot experiments in this study were performed independently for three times, and quantification results were generated based on all three repeats.

## Data availability

All data are contained within the article.

---

## References

1. Siegel, R. L., Miller, K. D., Fuchs, H. E., and Jemal, A. (2021) Cancer statistics, 2021. *CA: Cancer J. Clin.* **71**, 7–33
2. Miller, K. D., Nogueira, L., Mariotto, A. B., Rowland, J. H., Yabroff, K. R., Alfano, C. M., *et al.* (2019) (2019) Cancer treatment and survivorship statistics. *CA: Cancer J. Clin.* **69**, 363–385
3. Rusthoven, C. G., Jones, B. L., Flaig, T. W., Crawford, E. D., Koshy, M., Sher, D. J., *et al.* (2016) Improved survival with prostate radiation in addition to androgen deprivation therapy for men with newly diagnosed metastatic prostate cancer. *J. Clin. Oncol.* **34**, 2835–2842
4. Litwin, M. S., and Tan, H.-J. (2017) The diagnosis and treatment of prostate cancer: a review. *JAMA* **317**, 2532–2542
5. Lee, S. Y., Jeong, E. K., Ju, M. K., Jeon, H. M., Kim, M. Y., Kim, C. H., *et al.* (2017) Induction of metastasis, cancer stem cell phenotype, and oncogenic metabolism in cancer cells by ionizing radiation. *Mol. Cancer* **16**, 1–25
6. Steele, E. M., and Holmes, J. A. (2019) A review of salvage treatment options for disease progression after radiation therapy for localized prostate cancer. *Urol. Oncol. Semin. Original Invest.* **37**, 582–598
7. Wallis, C. J. D., Glaser, A., Hu, J. C., Huland, H., Lawrentschuk, N., Moon, D., *et al.* (2018) Survival and complications following surgery and radiation for localized prostate cancer: an international collaborative review. *Eur. Urol.* **73**, 11–20
8. Rhee, S. G. (2016) Overview on peroxiredoxin. *Mol. Cell* **39**, 1–5
9. Rhee, S. G., Chae, H. Z., and Kim, K. (2005) Peroxiredoxins: a historical overview and speculative preview of novel mechanisms and emerging concepts in cell signaling. *Free Radic. Biol. Med.* **38**, 1543–1552
10. Hampton, M. B., Vick, K. A., Skoko, J. J., and Neumann, C. A. (2018) Peroxiredoxin involvement in the initiation and progression of human cancer. *Antioxid. Redox Signal.* **28**, 591–608
11. Sies, H., and Jones, D. P. (2020) Reactive oxygen species (ROS) as pleiotropic physiological signalling agents. *Nat. Rev. Mol. Cell Biol.* **21**, 363–383
12. Kim, T. H., Song, J., Alcantara Llaguno, S. R., Murnan, E., Liyanarachchi, S., Palanichamy, K., *et al.* (2012) Suppression of peroxiredoxin 4 in glioblastoma cells increases apoptosis and reduces tumor growth. *PLoS One* **7**, e42818
13. Kim, T. H., Song, J., Kim, S.-H., Parikh, A. K., Mo, X., Palanichamy, K., *et al.* (2014) Piperlongumine treatment inactivates peroxiredoxin 4, exacerbates endoplasmic reticulum stress, and preferentially kills high-grade glioma cells. *Neuro. Oncol.* **16**, 1354–1364
14. Wei, Q., Jiang, H., Xiao, Z., Baker, A., Young, M. R., Veenstra, T. D., *et al.* (2011) Sulfiredoxin–peroxiredoxin IV axis promotes human lung cancer progression through modulation of specific phosphokinase signaling. *Proc. Natl. Acad. Sci. U. S. A.* **108**, 7004–7009
15. Palande, K. K., Beekman, R., van der Meeren, L. E., Beverloo, H. B., Valk, P. J. M., and Touw, I. P. (2011) The antioxidant protein peroxiredoxin 4 is epigenetically down regulated in acute promyelocytic leukemia. *PLoS One* **6**, e16340
16. Basu, A., Banerjee, H., Rojas, H., Martinez, S. R., Roy, S., Jia, Z., *et al.* (2011) Differential expression of peroxiredoxins in prostate cancer: Consistent upregulation of PRDX3 and PRDX4. *Prostate* **71**, 755–765
17. Yi, N., Xiao, M. B., Ni, W. K., Jiang, F., Lu, C. H., and Ni, R. Z. (2014) High expression of peroxiredoxin 4 affects the survival time of colorectal cancer patients, but is not an independent unfavorable prognostic factor. *Mol. Clin. Oncol.* **2**, 767–772
18. Demasi, A. P. D., Martinez, E. F., Napimoga, M. H., Freitas, L. L., Vassallo, J., Duarte, A. S. S., *et al.* (2013) Expression of peroxiredoxins I and IV in multiple myeloma: association with immunoglobulin accumulation. *Virchows Archiv.* **463**, 47–55
19. Zheng, J., Guo, X., Nakamura, Y., Zhou, X., Yamaguchi, R., Zhang, J., *et al.* (2020) Overexpression of PRDX4 modulates tumor microenvironment and promotes urethane-induced lung tumorigenesis. *Oxidative Med. Cell Longev.* **2020**, 8262730
20. Logothetis, C. J., and Lin, S.-H. (2005) Osteoblasts in prostate cancer metastasis to bone. *Nat. Rev. Cancer* **5**, 21–28
21. Rafiei, S., Tiedemann, K., Tabariès, S., Siegel, P. M., and Komarova, S. V. (2015) Peroxiredoxin 4: a novel secreted mediator of cancer induced osteoclastogenesis. *Cancer Lett.* **361**, 262–270
22. Grasso, C. S., Wu, Y.-M., Robinson, D. R., Cao, X., Dhanasekaran, S. M., Khan, A. P., *et al.* (2012) The mutational landscape of lethal castration-resistant prostate cancer. *Nature* **487**, 239–243
23. Kumar, A., Coleman, I., Morrissey, C., Zhang, X., True, L. D., Gulati, R., *et al.* (2016) Substantial interindividual and limited intraindividual genomic diversity among tumors from men with metastatic prostate cancer. *Nat. Med.* **22**, 369–378

24. Abida, W., Cyrta, J., Heller, G., Prandi, D., Armenia, J., Coleman, I., *et al.* (2019) Genomic correlates of clinical outcome in advanced prostate cancer. *Proc. Natl. Acad. Sci. U. S. A.* **116**, 11428–11436

25. Robinson, D., Van Allen, E. M., Eliezer, M., Wu, Y.-M., al., e., and Chinnaiyan, Arul M. (2015) Integrative clinical genomics of advanced prostate cancer. *Cell* **161**, 1215–1228

26. Cao, Z., Tavender, T. J., Roszak, A. W., Cogdell, R. J., and Bulleid, N. J. (2011) Crystal structure of reduced and of oxidized peroxiredoxin IV enzyme reveals a stable oxidized decamer and a non-disulfide-bonded intermediate in the catalytic cycle. *J. Biol. Chem.* **286**, 42257–42266

27. Fujii, J., Ikeda, Y., Kurahashi, T., and Homma, T. (2015) Physiological and pathological views of peroxiredoxin 4. *Free Radic. Biol. Med.* **83**, 373–379

28. Homma, T., Kurahashi, T., Ishii, N., Shirasawa, N., and Fujii, J. (2020) Testis-specific peroxiredoxin 4 variant is not absolutely required for spermatogenesis and fertility in mice. *Sci. Rep.* **10**, 1–12

29. Lonergan, P. E., and Tindall, D. J. (2011) Androgen receptor signaling in prostate cancer development and progression. *J. Carcinog.* **10**, 20

30. Tan, M. H. E., Li, J., Xu, H. E., Melcher, K., and Yong, E.-l. (2015) Androgen receptor: structure, role in prostate cancer and drug discovery. *Acta Pharmacol. Sin.* **36**, 3–23

31. Li, Q., Deng, Q., Chao, H.-P., Liu, X., Lu, Y., Lin, K., *et al.* (2018) Linking prostate cancer cell AR heterogeneity to distinct castration and enzalutamide responses. *Nat. Commun.* **9**, 3600

32. Corey, E., Quinn, J. E., Buhler, K. R., Nelson, P. S., Macoska, J. A., True, L. D., *et al.* (2003) LuCaP 35: a new model of prostate cancer progression to androgen independence. *Prostate* **55**, 239–246

33. Piccinini, F., Kiss, A., and Horvath, P. (2016) CellTracker (not only) for dummies. *Bioinformatics* **32**, 955–957

34. Khandrika, L., Kumar, B., Koul, S., Maroni, P., and Koul, H. K. (2009) Oxidative stress in prostate cancer. *Cancer Lett.* **282**, 125–136

35. Udensi, U. K., and Tchounwou, P. B. (2016) Oxidative stress in prostate hyperplasia and carcinogenesis. *J. Exp. Clin. Cancer Res.* **35**, 1–19

36. Hayes, J. D., Dinkova-Kostova, A. T., and Tew, K. D. (2020) Oxidative stress in cancer. *Cancer Cell* **38**, 167–197

37. Park, J. H., Kim, Y. S., Lee, H. L., Shim, J. Y., Lee, K. S., Oh, Y. J., *et al.* (2006) Expression of peroxiredoxin and thioredoxin in human lung cancer and paired normal lung. *Respirology* **11**, 269–275

38. Karihtala, P., Mäntyniemi, A., Kang, S. W., Kinnula, V. L., and Soini, Y. (2003) Peroxiredoxins in breast carcinoma. *Clin. Cancer Res.* **9**, 3418–3424

39. Gritsina, G., Gao, W.-Q., and Yu, J. (2019) Transcriptional repression by androgen receptor: roles in castration-resistant prostate cancer. *Asian J. Androl.* **21**, 215–223

40. Manning, B. D., and Toker, A. (2017) AKT/PKB signaling: navigating the network. *Cell* **169**, 381–405

41. Alessi, D. R., Andjelkovic, M., Caudwell, B., Cron, P., Morrice, N., Cohen, P., *et al.* (1996) Mechanism of activation of protein kinase B by insulin and IGF-1. *EMBO J.* **15**, 6541–6551

42. Alessi, D. R., James, S. R., Downes, C. P., Holmes, A. B., Gaffney, P. R. J., Reese, C. B., *et al.* (1997) Characterization of a 3-phosphoinositide-dependent protein kinase which phosphorylates and activates protein kinase Bα. *Curr. Biol.* **7**, 261–269

43. Stokoe, D., Stephens, L. R., Copeland, T., Gaffney, P. R. J., Reese, C. B., Painter, G. F., *et al.* (1997) Dual role of phosphatidylinositol-3,4,5-trisphosphate in the activation of protein kinase B. *Science* **277**, 567

44. Sarbassov, D. D., Guertin, D. A., Ali, S. M., and Sabatini, D. M. (2005) Phosphorylation and regulation of Akt/PKB by the rictor-mTOR complex. *Science* **307**, 1098

45. Yang, J., Cron, P., Good, V. M., Thompson, V., Hemmings, B. A., and Barford, D. (2002) Crystal structure of an activated Akt/Protein Kinase B ternary complex with GSK3-peptide and AMP-PNP. *Nat. Struct. Biol.* **9**, 940–944

46. Wu, D., and Pan, W. (2010) GSK3: a multifaceted kinase in wnt signaling. *Trends Biochem. Sci.* **35**, 161–168

47. Zhan, T., Rindtorff, N., and Boutros, M. (2017) Wnt signaling in cancer. *Oncogene* **36**, 1461–1473

48. Li, H.-X., Sun, X.-Y., Yang, S.-M., Wang, Q., and Wang, Z.-Y. (2018) Peroxiredoxin 1 promoted tumor metastasis and angiogenesis in colorectal cancer. *Pathol. Res. Pract.* **214**, 655–660

49. Stresing, V., Baltziskueta, E., Rubio, N., Blanco, J., Arriba, M., Valls, J., *et al.* (2013) Peroxiredoxin 2 specifically regulates the oxidative and metabolic stress response of human metastatic breast cancer cells in lungs. *Oncogene* **32**, 724–735

50. Chandrashekar, D. S., Bashel, B., Balasubramanya, S. A. H., Creighton, C. J., Ponce-Rodriguez, I., Chakravarthi, B., *et al.* (2017) Ualcan: a portal for facilitating tumor subgroup gene expression and survival analyses. *Neoplasia (New York, N.Y.)* **19**, 649–658

51. Li, Y., Ge, D., and Lu, C. (2019) The SMART App: an interactive web application for comprehensive DNA methylation analysis and visualization. *Epigenetics & Chromatin* **12**, 71

52. Messeguer, X., Escudero, R., Farré, D., Núñez, O., Martínez, J., and Albà, M. M. (2002) PROMO: detection of known transcription regulatory elements using species-tailored searches. *Bioinformatics* **18**, 333–334

53. Sanjana, N. E., Shalem, O., and Zhang, F. (2014) Improved vectors and genome-wide libraries for CRISPR screening. *Nat. Methods* **11**, 783–784

54. Franken, N. A. P., Rodermond, H. M., Stap, J., Haveman, J., and Van Bree, C. (2006) Clonogenic assay of cells *in vitro*. *Nat. Protoc.* **1**, 2315–2319

55. Darzynkiewicz, Z., and Juan, G. (1997) DNA content measurement for DNA ploidy and cell cycle analysis. *Curr. Protoc. Cytom.* https://doi.org/10.1002/0471142956.cy0705s00

56. Liang, C.-C., Park, A. Y., and Guan, J.-L. (2007) *In vitro* scratch assay: a convenient and inexpensive method for analysis of cell migration *in vitro*. *Nat. Protoc.* **2**, 329–333

57. Kramer, N., Walzl, A., Unger, C., Rosner, M., Krupitza, G., Hengstschläger, M., *et al.* (2013) *In vitro* cell migration and invasion assays. *Mutat. Res.* **752**, 10–24

58. Kalyanaraman, B., Darley-Usmar, V., Davies, K. J. A., Dennery, P. A., Forman, H. J., Grisham, M. B., *et al.* (2012) Measuring reactive oxygen and nitrogen species with fluorescent probes: challenges and limitations. *Free Radic. Biol. Med.* **52**, 1–6

59. Grasso, C. S., Wu, Y.-M., Robinson, D. R., and Tomlins, S. A. (2012) The mutational landscape of lethal castration-resistant prostate cancer. *Nature* **487**, 239–243

60. The ICGC/TCGA Pan-Cancer Analysis of Whole Genomes Consortium (2020) Pan-cancer analysis of whole genomes. *Nature* **578**, 82–93

61. The Cancer Genome Atlas Research Network (2017) Integrated genomic characterization of oesophageal carcinoma. *Nature* **541**, 169–175